Modeling and Optimization of THz Photoconductive Antenna

Nimisha Arora[1], Aparajita Bandyopadhyay[2], Amartya Sengupta[1]

[1]Department of Physics, Indian Institute of Technology Delhi, New Delhi, India
[2]DRDO-JATC, Indian Institute of Technology Delhi, New Delhi, India
*Corresponding author: nimishaarora051996@gmail.com

Abstract: This work presents a computational approach to model efficient terahertz photoconductive antennas. Two configurations have been proposed and optimized using RF module and further verified using wave optics module present in commercially available finite element method solver COMSOL Multiphysics. For this optimized configuration, optical response has been simulated for femtosecond optical pulse excitation. Semiconductor module is then utilized to study electrical response of the 2D THz-PCA. The obtained results support the efficient generation of THz-PCA by observing transient current collected at the terminals of the electrode, addressing the problem of low output power of THz PCA.

Keywords: Terahertz, photoconductive antenna, subpicosecond

INTRODUCTION:

The Terahertz (THz) range of frequencies lies in the transitional region between the classically described electronics region (<100 GHz) and the photonics region (>10 THz), where quantum nature of light dominates over wave nature [1]. Approaching the THz regime from either of these regimes comes with their unique challenges. For instance, increasing the operating frequency of the microwave devices is limited by the carrier mobility of the oscillating semiconductor material [2]; whereas, reducing the energy of the emitted photon generated by electronic transitions in a semiconductor is limited by the fact that the thermal energy at room temperature is larger than THz energy [3]. THz waves have potential applications in many areas. For example, semiconductor phonons vibrations [4]; unique fingerprint lines of macrobiomolecules, pharmaceuticals, narcotics, and explosives [5-8]. This technique is also effectively used in the quality control of electronics fabrication and packaging [9-14] as well as composite material inspection [15], biomedical imaging [16-18], burn wound assessment [19, 20], and dental tissue imaging [21]. The objecti-

ve of this work is to computationally optimize a novel THz-photo conductive antenna (THz-PCA) design with enhanced optical-to-THz conversion efficiency. It has been done by utilizing the commercially available finite element method (FEM) solver COMSOL Multiphysics. The paper is organized as follows: Section 2 introduces the theory and concept behind the proposed THz-PCA design, section 3 defines the Computational modeling and methodology, and section 4 includes the simulation results.

THEORY OF THz PHOTOCONDUCTIVE ANTENNA:

The understanding of THz pulse emission from PCA incorporates the electrical response of photoconductive material triggered by an optical pulse. Figure 1 demonstrates the THz emission mechanism with time propagation with an incident subpicosecond pulse (<1ps). Figure 2 represents a 3-dimensional isometric view of THz-PCA. It show the main components which include the photoconductive substrate, high resistivity float zone silicon (HRFZ-Si) on the back of the substrate, and THz dipole antenna electrode fabricated on top of the substrate
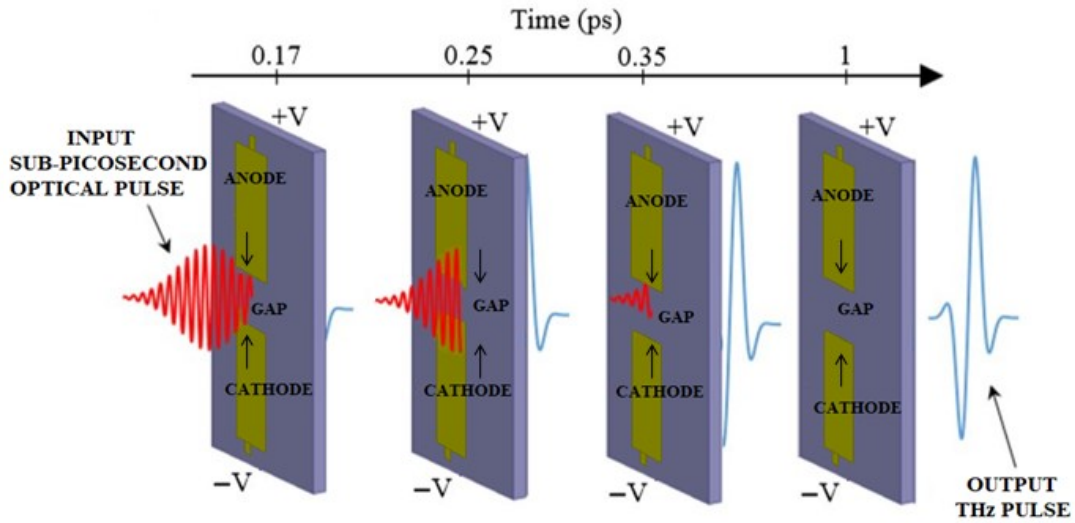
Figure 2: Illustration of pulsed THz generation in a PCA. Femtosecond optical pulse propagates into the photoconductor, generates a transient photocurrent, which drives the antenna, and is re-emitted as a broadband THz pulse.
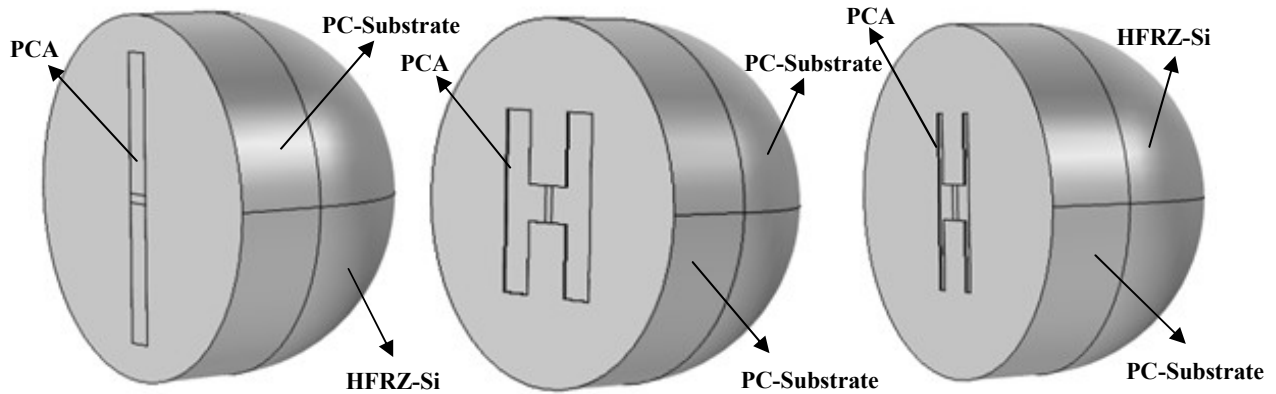
Figure 1: (A) Strip Dipole Antenna (B, C) Hertzian Dipole Antenna

with an external DC bias. Generated free photocarriers after optical excitation, are accelerated towards these dipole electrodes which results in a transient photocurrent [22, 23]. The rise time of the photocurrent is proportional to the rise time of the incident pulse and the decay time of the photocurrent depends on the electrical properties of the photoconductive material used [24]. Hence, it is very critical to choose the appropriate photoconductive material having carrier lifetime of few picoseconds and low temperature grown Gallium Arsenide (LT-GaAs) [25-27] is one of the ideal materials. Most of

the optical energy that is converted into the generated broadband THz pulse is directed by the antenna and is proportional to the transient photocurrent collected at the terminals of the electrode. Emitted THz pulse is detected either through the use of a calibrated THz power detectors (bolometer and pyroelectric detectors) [28, 29] or by an electro-optic sampling of the THz pulse in a time-domain spectroscopy (TDS) [30]. It measures the temporal profile of the THz pulse with a high signal to noise ratio (SNR). The emitted broadband THz pulse can be described by electric field expression:

$$E_{THz}(r,t) = -\frac{1}{4\pi\epsilon_0 c^2}\frac{\partial}{\partial t}\int \frac{J_s\left(r',t-\frac{|r-r'|}{c}\right)}{|r-r'|}ds' \qquad (1)$$

Where, J_s is spatially and time dependent surface current density.

DESIGNING AND COMPUTATIONAL MODELING OF THz PCA:

For the purpose of computational modeling, two different antenna designs have been modeled and optimized for different antenna parameters (Figs. 2(A), 2(B), and 2(C)). The optimized THz-PCAs and its radiation patterns were verified using two models (RF & Wave optics) present in commercially available finite element method solver COMSOL software. The detailed computational study is structured in flowchart as shown in Fig. 3:
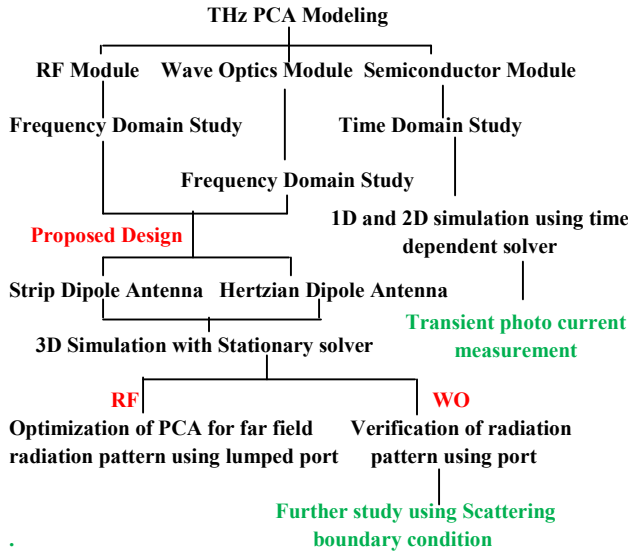
Figure 3: Flow chart of computational modeling.

It is evident from the flowchart that computational modeling is divided into three steps, (1) Optimization of the antenna structure using RF module and further verified by wave optics module; (2) For this optimized structure, calculating the optical response using the spatial distribution of optical field; (3) Finding the electrical response in the 2D structure by solving coupled time-dependent Poisson's and drift-diffusion equation. The simulation is divided into three parts:

1) OPTIMIZATION:

Antenna structures (Figs. 2(A), 2(B), and 2(C)) were first optimized using RF module and then using wave optics module. Material properties used for this, are listed in Table 1:

Table 1: Material properties used during optimization

Material Property	Unit (SI)	Au	LT-GaAs	Si	Air
Relative permeability	1	1	1	1	1
Relative permittivity	1	-22.5	12.9	11.7	1
Electrical conductivity	S/m	2400	1000	1.5e-6	1.4e-11

The lens material was index-matched to the substrate (n~3.4) to reduce multi-reflections. This also helps to decrease the divergence of THz radiation which results in increased gain [31]. PCA is then optimized for various parameters as length, gap size, and thickness etc. with an impedance matched condition on the antenna.

2) OPTICAL RESPONSE:

It was determined by solving the electromagnetic wave equation in the frequency domain:

$$\Delta \times \mu_r^{-1}\left(\Delta \times \vec{E}\right) - k_0^2\left(\epsilon_r - \frac{j\lambda\sigma}{2\pi c\epsilon_r}\right)\vec{E} = 0 \qquad (2)$$

Here, ϵ_r, σ, and μ_r are the relative permittivity, conductivity, and relative permeability of the material respectively, k_0 and ϵ_0 are the free space propagation constant and permittivity respectively, λ is the excitation wavelength, c is the speed of light in vacuum, and $\vec{E}$ is the electric field vector. Optical excitation in the gap was defined by a subpicosecond pulse of Gaussian dependence along x and y-axis with

$$E_{inc} = \hat{a}_e E_o \exp\left(2\ln(0.5)\frac{(x-x_o)^2}{D_x^2}\right)\exp\left(2\ln(0.5)\frac{(y-y_o)^2}{D_y^2}\right), \qquad (3)$$

polarization along $\hat{a}_e$. x_0 and y_0 represent the location of the optical beam. D_x and D_y are the half power beam widths (HPBW) along the x and y-axis respectively. The electric field amplitude E_0 corresponds to the peak electric field of the

subpicosecond pulse optical excitation and it can be approximated as:

$$E_0 = \sqrt{\frac{P_{ave}8\eta_0}{f_p D_x D_y D_t}} \left(-\frac{\ln(0.5)}{\pi}\right)^{\frac{3}{4}} \qquad (4)$$

Here, f_p, P_{ave}, η_0, and D_t are the pulse repetition rate, average laser power, free-space wave impedance, and pulse time duration respectively. In this part of the simulation, $\vec{E}$ was found everywhere in the computational domain. Similarly, total power flux density distribution in the computational domain can also be derived from electric field distribution as follows:

$$P_s(x,y,z) = \left(|P_x(x,y,z)|^2 + |P_y(x,y,x)|^2 + |P_{z(x,y,z)}|^2\right) \qquad (5)$$

Analogically, P_y and P_z can be written.

3) ELECTRICAL RESPONSE:

This step of the simulation utilized the standard time-domain form of the coupled Poisson's (6) and drift-diffusion (7, 8) equations:

$$\epsilon_0 \nabla.(\epsilon_r \nabla V) = q(n - p - N_D + N_A), \qquad (6)$$

$$\frac{\partial n}{\partial t} = -\frac{1}{q}\nabla.\left\{-\mu_n q\nabla(V+\chi)n + \mu_n k_b TG\left(\frac{n}{N_c}\right)\nabla n\right\} - r(x,y,z) + g(x,y,z,t), \qquad (7)$$

$$\frac{\partial p}{\partial t} = \frac{1}{q}\nabla.\left\{-\mu_p q\nabla(V+\chi+E_g)p + \mu_p k_b TG\left(\frac{p}{N_v}\right)\nabla p\right\} - r(x,y,z) + g(x,y,z,t) \qquad (8)$$

Here, V, n, and p are input variables. Last two terms in Eqs. (7) and (8) stand for recombination and generation of carriers. Carrier recombination was described by Schottky-Read-Hall (9) and Auger recombination models (10).

$$r_{SRH}(x,y,z) = \frac{np - \gamma_n\gamma_p n_{i,eff}^2}{(\tau_p(n+n_1) + \tau_n(p+p_1))},$$

$$n_1 = \gamma_n n_{i,eff}\exp\left(\frac{\Delta E_t}{k_b T}\right), \; p_1 = \gamma_p n_{i,eff}\exp\left(\frac{\Delta E_t}{k_b T}\right), \quad (9)$$

$$r_{AR}(x,y,z) = (C_n n + C_p p)\left(np - \gamma_n\gamma_p n_{i,eff}^2\right), \qquad (10)$$

For the electrical response, only LT-GaAs layer was considered. The last term in Eqs. (7) and (8) implied

generated photocarriers due to optical response obtained in step 2. All the physical quantities necessary for THz-PCA modeling that appeared in Eqs. (3)-(10) are tabulated in the Table 2:

Table 2: Electrical, optical properties, and constants used in simulation.

| Symbol	Description	Units	Value
ϵ_r	LT-GaAs	None	12.9
N_D	Donor doping concentration	1/cm^3	1e16
N_A	Acceptor doping concentration	1/cm^3	0
μ_n	Electron mobility	m^2/V/s	0.8
μ_p	Hole mobility	m^2/V/s	0.047
E_g	Bandgap	V	1.424
χ	Electron affinity	V	4.07
T	Room temperature	K	300
τ_n	SRH electron lifetime	s	480e-12
τ_p	SRH hole lifetime	s	480e-12
C_n	Auger electron coefficient	cm^6/s	7e-30
C_p	Auger hole coefficient	cm^6/s	7e-30
$n_{i,eff}$	Effective intrinsic carrier concentration	1/m^3	1.23e-12
V_{bias}	Bias Voltage	V	30
λ	Free space wavelength	nm	800
P_{ave}	Average laser power	mW	3.57
f_p	Laser pulse repetition rate	MHz	80
x_0	Pulse x-axis center location	μm	0
y_0	Pulse y-axis center location	μm	0
t_0	Pulse center location (time)	ps	2
D_x	Pulse HPBW (x direction)	μm	3
D_y	Pulse HPBW (y direction)	μm	3
D_t	Pulse FWHM (time)	fs	133
k_{pc}	Photoconductor extinction coefficient of LT-GaAs	None	0.0625
$\hat{a}_e$	E_{inc} polarization unit vector	None	$\hat{a}_x$

RESULT AND DISCUSSION:

Dipole Antenna and Hertzian Antenna (Figs. 2(A), 2(B), and 2(C)) were first optimized for its length, thickness, and gap parameter in RF module. For the optimization of THz-PCA (Fig. 2(A)) at 1 THz, arm length is varied from 75 μm to 100 μm, thickness is varied from 15 μm to 20 μm, and the gap is varied

from 2 μm to 10 μm. And, for THz-PCA (Figs. 2(B) and 2(C)), length is varied from 75 μm to 100 μm, the thickness is varied from 20 μm to 60 μm, and the gap is varied from 2 μm to 10 μm. Table 3 defines the parameters value obtained during optimization.

Table 3: Simulated parameter values for Optimized THz PCA design for Figs. 2 (A), 2(B), and 2(C).

| THz-PCA Parameter	Strip dipole antenna, Fig. 2(A)	Hertzian dipole antenna, Fig. 2(B)	Hertzian dipole antenna, Fig. 2(C)
$l_{antenna}(\mu m)$	75.76	93.46	300, 37.5b/w strip
$r_{antenna}(\mu m)$	19.74	20, monotonic increase with r	20, monotonic increase
$gap_{size}(\mu m)$	5	6, monotonic increase with g	3.75
Directivity(dB)	2.9619	3.0019	2.8052

Observed far-field THz radiation pattern for optimized THz-PCA design is shown in Fig. 4.
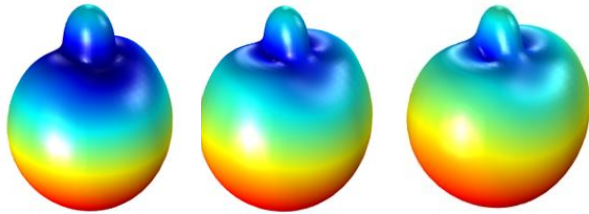
Figure 4: Far-field THz radiation pattern for optimized antenna design, shown in Figs. 2 (A), (B), and (C)

The blue bump in the figure shows that the radiation is also emitted across the PCA towards the HRFZ-Si ball lens, in the form of a narrow beam. It is advantageous to have this sort of radiation pattern as it allows the incidence of the subpicosecond optical pulse in one direction and receive the THz pulse on the other side of the PCA. This observed far-field THz radiation pattern is then validated by the wave-optics module. To find an optical response of the THz-PCA, a subpicosecond pulse of Gaussian distribution along x and y-axis with polarization along the x-axis is incident on the gap with parameters listed in the Table 2. Figure 5

demonstrates the simulated results in wave-optics module to study optical response of optimized PCA design:
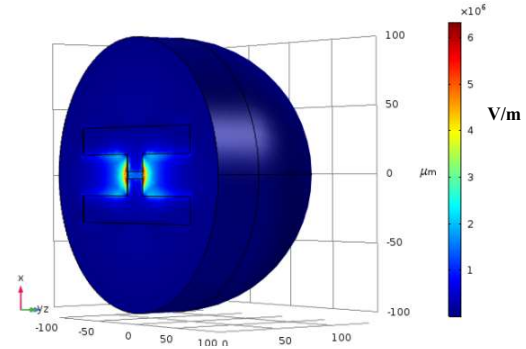

Figure 5: optical response PCA design shown in figure 2 (B) in wave optics module

Figure 6 represents the far-field radiation pattern for the THz-PCAs.
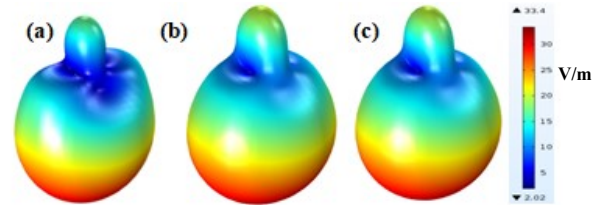
Figure 6: 3-dimensional far-field radiation pattern for optical subpiceseconds excitation corresponding to PCA designs shown in Figs. 2 (A), 2(B), and 2(C).

A narrow beam across the Si lens is observed with corresponding directivity value 3.610 dB, 5.223 dB, and 5.703 dB. Similar results were found for PCA designs shown in Figs. 2(A) and 2(C). The electric field distribution in Fig. 5 is used to study electrical response of THz-PCA using semiconductor module in 1D and 2D as discussed in section 2.3. Measured transient photocurrent for 2D PCA structure is shown below in Fig. 7. Evidently, most of the carrier generation occurs in the gap and those generated far from the electrode recombine due to short carrier lifetime and do not account into transient photocurrent. THz-PCA is an integral step in THz time- domain imaging and spectroscopy technology. Computational modeling can be a valuable tool for researchers as it allows the device performance to be predicted before expensive and time-consuming prototyping and testing. Future work is ongoing to
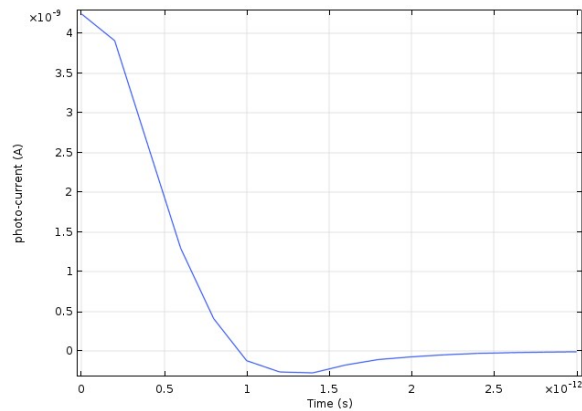
Figure 7: Transient photocurrent measured in time dependent semiconductor module in 2D computational domain for carrier recombination time of 480 ps.

develop full 3-dimensional computation using FEM COMSOL solver.

REFERENCES:

1) Fattinger, C., & Grischkowsky, D. (1989). THz beams. *Applied Physics Letters*, *54*(6), 490-492.

2) Samoska, L. A. (2011). An overview of solid-state integrated circuit amplifiers in the submillimeter-wave and THz regime. *IEEE Transactions on THz Science and Technology*, *1*(1), 9-24.

3) Dean, P., Valavanis, A., Keeley, J., Bertling, K., Lim, Y. L., Alhathlool, R., ... & Taimre, T. (2014). THz imaging using quantum cascade lasers—a review of systems and applications. *Journal of Physics D: Applied Physics*, *47*(37), 374008.

4) Cho, G. C., Han, P. Y., & Zhang, X. C. (1999, August). Time-resolved THz phonon spectroscopy in semiconductors. In *Lasers and Electro-Optics, 1999. CLEO/Pacific Rim'99. The Pacific Rim Conference on* (Vol. 3, pp. 789-790). IEEE.

5) Sushko, O., Dubrovka, R., & Donnan, R. S. (2013). THz spectral domain computational analysis of hydration shell of proteins with increasingly complex tertiary structure. *The Journal of Physical Chemistry B*, *117*(51), 16486-16492.

6) Kemp, M. C., Taday, P. F., Cole, B. E., Cluff, J. A., Fitzgerald, A. J., & Tribe, W. R. (2003, July). Security applications of THz technology. In *THz for Military and Security Applications* (Vol. 5070, pp. 44-53). International Society for Optics and Photonics.

7) Federici, J. F., Schulkin, B., Huang, F., Gary, D., Barat, R., Oliveira, F., & Zimdars, D. (2005). THz imaging and sensing for security applications—explosives, weapons and drugs. *Semiconductor Science and Technology*, *20*(7), S266.

8) Liu, H. B., Zhong, H., Karpowicz, N., Chen, Y., & Zhang, X. C. (2007). THz spectroscopy and imaging for defense and security applications. *Proceedings of the IEEE*, *95*(8), 1514-1527.

9) Jeon, T. I., & Grischkowsky, D. (1998). Characterization of optically dense, doped semiconductors by reflection THz time domain spectroscopy. *Applied Physics Letters*, *72*(23), 3032-3034.

10) Yamashita, M., Otani, C., Kawase, K., Nikawa, K., & Tonouchi, M. (2008). Noncontact inspection technique for electrical failures in semiconductor devices using a laser THz emission microscope. *Applied Physics Letters*, *93*(4), 041117.

11) Yamashita, M., Otani, C., Matsumoto, T., Midoh, Y., Miura, K., Nakamae, K., ... & Tonouchi, M. (2011). THz emission characteristics from p/n junctions with metal lines under non-bias conditions for LSI failure analysis. *Optics Express*, *19*(11), 10864-10873.

12) Minkevicius, L., Suzanoviciene, R., Balakauskas, S., Molis, G., Krotkus, A., Valusis, G., & Tamosiunas, V. (2012). Detection of tab wire soldering defects on silicon solar cells using THz time-domain spectroscopy. *Electronics letters*, *48*(15), 932-934.

13) Burford, N. M., El-Shenawee, M. O., O'neal, C. B., & Olejniczak, K. J. (2014). THz imaging for nondestructive evaluation of packaged power electronic devices. *Int. J. Emerg. Technol. Adv. Eng*, *4*(1), 395-401.

14) Kiwa, T., Tonouchi, M., Yamashita, M., & Kawase, K. (2003). Laser terahertz-emission

microscope for inspecting electrical faults in integrated circuits. *Optics letters*, *28*(21), 2058-2060.

15) Ospald, F., Zouaghi, W., Beigang, R., Matheis, C., Jonuscheit, J., Recur, B., ... & González, L. V. (2013). Aeronautics composite material inspection with a THz time-domain spectroscopy system. *Optical Engineering*, *53*(3), 031208.

16) Ashworth, P. C., Pickwell-MacPherson, E., Provenzano, E., Pinder, S. E., Purushotham, A. D., Pepper, M., & Wallace, V. P. (2009). THz pulsed spectroscopy of freshly excised human breast cancer. *Optics express*, *17*(15), 12444-12454.

17) Bowman, T. C., El-Shenawee, M., & Campbell, L. K. (2015). THz imaging of excised breast tumor tissue on paraffin sections. *IEEE Transactions on Antennas and Propagation*, *63*(5), 2088-2097.

18) Hassan, A. M., Hufnagle, D. C., El-Shenawee, M., & Pacey, G. E. (2012, June). THz imaging for margin assessment of breast cancer tumors. In *Microwave Symposium Digest (MTT), 2012 IEEE MTT-S International* (pp. 1-3). IEEE.

19) Taylor, Z. D., Singh, R. S., Culjat, M. O., Suen, J. Y., Grundfest, W. S., Lee, H., & Brown, E. R. (2008). Reflective THz imaging of porcine skin burns. *Optics letters*, *33*(11), 1258-1260.

20) Wilmink, G. J., Ibey, B. L., Rivest, B. D., Grundt, J. E., Roach, W. P., Tongue, T. D., ... & Cerna, C. Z. (2011). Development of a compact THz time-domain spectrometer for the measurement of the optical properties of biological tissues. *Journal of biomedical optics*, *16*(4), 047006.

21) Crawley, D. A., Longbottom, C., Wallace, V. P., Cole, B. E., Arnone, D. D., & Pepper, M. (2003). Three-dimensional THz pulse imaging of dental tissue. *Journal of Biomedical Optics*, *8*(2), 303-308.

22) Auston, D. H. (1983). Subpicosecond electro-optic shock waves. *Applied Physics Letters*, *43*(8), 713-715.

23) Auston, D. H., Cheung, K. P., & Smith, P. R. (1984). Picosecond photoconducting Hertzian dipoles. *Applied physics letters*, *45*(3), 284-286.

24) Moreno, E., Pantoja, M. F., Garcia, S. G., Bretones, A. R., & Martin, R. G. (2014). Time-domain numerical modeling of THz photoconductive antennas. *IEEE Transactions on THz Science and Technology*, *4*(4), 490-500.

25) Tani, M., Sakai, K., Abe, H., Nakashima, S. I., Harima, H., Hangyo, M., & Tsukada, N. (1994). Spectroscopic characterization of low-temperature grown GaAs epitaxial films. *Japanese journal of applied physics*, *33*(9R), 4807.

26) Moon, K., Choi, J., Shin, J. H., Han, S. P., Ko, H., Kim, N., ... & Park, K. H. (2014). Generation and Detection of THz Waves Using Low-Temperature-Grown GaAs with an Annealing Process. *ETRI Journal*, *36*(1), 159-162.

27) Salem, B., Morris, D., Aimez, V., Beerens, J., Beauvais, J., & Houde, D. (2005). Pulsed photoconductive antenna THz sources made on ion-implanted GaAs substrates. *Journal of Physics: Condensed Matter*, *17*(46), 7327.

28) Yang, S. H., Hashemi, M. R., Berry, C. W., & Jarrahi, M. (2014). 7.5% optical-to-THz conversion efficiency offered by photoconductive emitters with three-dimensional plasmonic contact electrodes. *IEEE Transactions on THz Science and Technology*, *4*(5), 575-581.

29) Auston, D. H., Cheung, K. P., & Smith, P. R. (1984). Picosecond photoconducting Hertzian dipoles. *Applied physics letters*, *45*(3), 284-286.

30) Auston, D. H., Cheung, K. P., Valdmanis, J. A., & Kleinman, D. A. (1984). Cherenkov radiation from femtosecond optical pulses in electro-optic media. *Physical Review Letters*, *53*(16), 1555.

31) Liu, H., Yu, J., Huggard, P., & Alderman, B. (2013). A multichannel THz detector using integrated bow-tie antennas. *International Journal of Antennas and Propagation*, *2013*.